processes

MDPI

Article

Fractional Modeling of Coupled Heat and Moisture Transfer with Gas-Pressure-Driven Flow in Raw Cotton

Normakhmad Ravshanov [1] and Istam Shadmanov [2,*]

[1] Modelling of Complex Systems Department, Digital Technologies and Artificial Intelligence Research Institute, Boz-2 St. 17A, Tashkent 100125, Uzbekistan
[2] Department of Information Systems and Digital Technologies, Bukhara State University, M. Ikbol St. 11, Bukhara 200114, Uzbekistan
* Correspondence: i.u.shadmanov@buxdu.uz

Abstract

This study introduces a multidimensional mathematical model and a robust numerical algorithm with second-order accuracy for modeling the complex coupled processes of heat and moisture transfer with gas-pressure-driven flow, based on time-fractional differential equations (with Caputo derivatives of order $0 < \alpha \leq 1$), which capture the memory effects and anomalous diffusion inherent in heterogeneous porous media. The proposed model integrates conductive and convective heat transfer; moisture diffusion and phase change; and pressure dynamics within the pore space and their bidirectional couplings. It also incorporates environmental interactions through boundary conditions for heat and moisture exchange with the ambient air; internal heat and moisture release; transient influx of solar radiation; and material heterogeneity, where all transport coefficients are spatially variable functions. To solve this nonlinear and coupled system, we developed a high-order, stable finite-difference scheme. The numerical algorithm employs an alternating direction-implicit approach, which ensures computational efficiency while maintaining numerical stability. We demonstrate the algorithm's capability through numerical simulations that monitor and predict the spatiotemporal evolution of coupled transport temperature, moisture content, and pressure fields. The results reveal how heterogeneity, diurnal solar radiation, and internal sources create localized hot spots, moisture accumulation zones, and pressure gradients that significantly influence the overall dynamics of storage and drying processes.

Keywords: coupled heat and mass transfer; moisture diffusivity; quality retention; drying methods; Caputo derivatives; heterogeneity; cotton raw

Check for updates

Academic Editor: Iqbal M. Mujtaba

Received: 4 January 2026
Revised: 16 January 2026
Accepted: 28 January 2026
Published: 29 January 2026

Copyright: © 2026 by the authors. Licensee MDPI, Basel, Switzerland. This article is an open access article distributed under the terms and conditions of the Creative Commons Attribution (CC BY) license.

1. Introduction

The coupled transport of heat and mass within heterogeneous porous media with pressure effects (pressure gradients in the pore space drive convective flow and influence moisture redistribution and heat transfer) is a fundamental physical process with profound implications across a diverse range of scientific and engineering disciplines. The accurate prediction of coupled heat–moisture transfer with gas-pressure-driven flow changes is crucial for optimizing efficiency, ensuring product quality retention, and preventing structural failures such as rotting in processes like storing and drying foodstuffs, agricultural products, and building materials [1–3]. The results of such studies can provide qualitatively new knowledge about the processes under study and more accurate forecasts of changes in indicators such as temperature and humidity, with the aim of optimizing the storage and

 https://doi.org/10.3390/pr14030481

processing conditions of agricultural raw materials. The complexity of these processes increases in heterogeneous porous materials, where variations in pore structure, composition, and thermophysical properties lead to localized, non-uniform transport pathways. Simple averaged models cannot adequately describe these variations.

The theoretical foundation for analyzing coupled transport phenomena was established in the mid-20th century. The groundbreaking work of Philip and De Vries [4] formulated a system of partial differential equations (PDEs) that connect temperature and moisture gradients. This system was later expanded by Luikov [5] into a comprehensive thermomechanical theory, adding pressure gradients. Liu et al. [6] proposed an analytical method for solving Luikov's system of heat and mass transfer equations with linearly time-dependent boundary conditions, ignoring the pressure gradient. However, Pandey et al. [7], focusing on the most general type of boundary conditions, used an eigenvalue analysis approach obtained using matrix calculus. A specific example of contact drying of a wet porous sheet with a uniform initial temperature and moisture distribution is considered. The classical models, based on integer-order Fickian and Fourier laws, were successfully applied to many problem areas [8]. Whitaker's volume-averaging approach [9] provided a rigorous method for deriving macroscopic transport equations from pore-scale physics to the theory of the drying method. However, they often do not account for "anomalous" or non-Fickian diffusion, long-term memory effects, internal heat–moisture release, and waiting time distributions frequently observed in complex heterogeneous porous media [10].

Considering pressure dynamics adds a crucial third dimension to the coupled transfer problem. In heterogeneous porous media, pressure gradients driven by phase changes, thermal expansion, and external loading can be a factor influencing moisture motion [11]. The convective flows generated by these pressure gradients significantly alter the rates of coupled heat–mass transfer, which is a key aspect of studying convection in heterogeneous porous materials [12,13]. Thanks to the efforts of these and many other scientists, significant theoretical and applied results have already been obtained, enabling a comprehensive study of heat and moisture exchange processes for raw cotton, including the Mamatov and Parpilev models [14], which provide an integer-order framework for describing the evolution of temperature and moisture under specified environmental conditions. However, under open-air storage, cotton piles are subjected to strongly time-varying ambient forces and exhibit non-ideal transport behavior associated with heterogeneous pore structures and history-dependent effects. Therefore, in this study, we extend the classical framework by introducing a time-fractional (Caputo) formulation, and we apply it to a 3D cotton pile under realistic boundary conditions (including solar/ambient effects). Furthermore, in [15], a mathematical model based on Fick's diffusion theory, Fourier's law of thermal conductivity, and thermoelastic mechanics was presented for analyzing the spatiotemporal distribution of moisture, temperature, and stress during the drying process. Ignoring this coupling, as many mathematical models do, can lead to substantial errors in predicting drying rates or moisture accumulation in long-term storage. Furthermore, real-world materials are rarely homogeneous. In references [16,17], advanced mathematical modeling techniques were employed to describe these phenomena with greater accuracy. From a numerical standpoint, solving PDEs with variable coefficients demands robust and efficient algorithms [18].

In this regard, fractional calculus and modeling have been powerful tools to address these limitations, and active research is underway to further develop mathematical modelling methodology to address a range of issues related to the storage and processing of agricultural products. By introducing derivatives of non-integer order, fractional differential equations (FDEs) effectively incorporate spatial non-locality and temporal memory into the

constitutive laws of coupled transport [19,20]. In [21], the application of fractional operators to physical problems was systematized and their intrinsic connection to continuous-time random walks was demonstrated, providing physical justification for their use in modeling anomalous diffusion. Despite this progress, the application of fractional calculus to the fully coupled problem of simultaneous heat, moisture, and pressure transport in heterogeneous porous media remains notably underdeveloped. Most existing fractional mathematical models focus on a single transport problem or a simplified two-phase coupling process [22]. Compared with the classical integer-order formulation for coupled heat–moisture transfer equations [23–25], their fractional-order (Caputo) counterparts are more complex due to the non-local nature of the derivatives, which predicts moisture redistribution rates that are 25–30% slower, indicates temperature persistence in critical zones lasting 15–20% longer, and offers enhanced temporal and computational cost estimations in forecasting thermal escalation events. This complexity necessitates the storage and summation of the entire time history [24,26]. Recent advancements in numerical methods for FDEs, such as those proposed in references [27,28], offer valuable tools. Adapting these methods to large-scale, nonlinear, multi-physics systems in three spatial dimensions remains a challenging and active area of research.

In this paper, we present a novel mathematical model and an associated numerical algorithm for the processes of joint heat and moisture transfer with gas flow in heterogeneous porous bodies. The model presents a system of three-dimensional, time-fractional Des to capture memory and anomalous diffusion, with spatially variable coefficients. We introduce a time-fractional formulation based on the Caputo derivative to model the moisture–heat evolution in raw cotton storage. The fractional order ($0 < \alpha \leq 1$) provides an additional degree of freedom to represent memory effects and anomalous (non-Fickian) transport arising from the porous, heterogeneous structure of raw cotton and the storage environment. It incorporates key physical mechanisms: conductive and convective transport, internal heat and moisture release (phase change; biological self-heating), and time-dependent boundary conditions representing environmental exchange and solar radiation influx. To solve this challenging coupled system, a second-order, stable finite-difference scheme based on an ADI (alternating direction-implicit) approach was developed, which is stable and time-efficient. We demonstrate the numerical algorithm's capability to simulate complex transport dynamics, providing a predictive tool with applications in drying and the long-term storage of agricultural food products.

2. Materials and Methods

The physical system under consideration is a three-dimensional, heterogeneous, porous body occupying a domain $\Omega \subset \mathbb{R}^3$ with boundary $\partial\Omega$. The body is exposed to a time-varying external environment, leading to the complex coupled transport of thermal energy (heat), liquid moisture, and gaseous pressure within its pore space. The primary objective is to develop a predictive mathematical model capable of accurately describing the spatiotemporal evolution of the temperature $T(\aleph, t)$, moisture content $M(\aleph, t)$, and pressure $P(\aleph, t)$ fields, accounting for the material's inherent heterogeneity and memory effects.

To capture the non-Fickian diffusion and hereditary properties observed in disordered porous media, we abandon the classical integer-order time derivative. Instead, we employ the Caputo fractional derivative of order α $(0 < \alpha \leq 1)$, defined as

$$\frac{\partial^\alpha f(t)}{\partial t^\alpha} = \frac{1}{\Gamma(1-\alpha)} \int_0^t \frac{f'(\xi) d\xi}{(t-\xi)^\alpha}$$

where $\Gamma(\cdot)$ is the Gamma function [29].

The coupled transport processes are governed by the following system of time-fractional partial differential equations:

Heat transfer equation depending on humidity and pressure:

$$\frac{\partial^\alpha T}{\partial t^\alpha} = \nabla \cdot (a_{11}(\aleph)\nabla T) + \nabla \cdot (a_{12}(\aleph)\nabla M) + \nabla \cdot (a_{13}(\aleph)\nabla P) + Q_T(\aleph, t) + S_R(\aleph, t), \quad (1)$$

where $a_{11}(\aleph)$ is the effective thermal conductivity tensor; the terms $\nabla \cdot (a_{12}(\aleph)\nabla M)$ and $\nabla \cdot (a_{13}(\aleph)\nabla P)$ represent the coupled fluxes of heat driven by moisture and pressure gradients; $Q_T(\aleph, t)$ denotes internal heat release (it is an assumed effective source to represent observed self-heating); and $S_R(\aleph, t)$ is a source term representing the absorption of solar radiation, which may vary diurnally.

Moisture transfer equation depending on temperature and pressure:

$$\frac{\partial^\alpha M}{\partial t^\alpha} = \nabla \cdot (a_{21}(\aleph)\nabla M) + \nabla \cdot (a_{22}(\aleph)\nabla T) + \nabla \cdot (a_{23}(\aleph)\nabla P) + Q_M(\aleph, t), \quad (2)$$

where $a_{21}(\aleph)$ is the moisture diffusivity tensor; the terms $\nabla \cdot (a_{22}(\aleph)\nabla T)$ and $\nabla \cdot (a_{23}(\aleph)\nabla P)$ account for moisture flux due to thermal gradients and pressure gradients; and $Q_M(\aleph, t)$ is internal moisture release.

Pressure dynamics equation depending on temperature and moisture content [5]:

$$\frac{\partial^\alpha P}{\partial t^\alpha} = \nabla \cdot (a_{31}(\aleph)\nabla P) + \nabla \cdot (a_{32}(\aleph)\nabla T) + \nabla \cdot (a_{33}(\aleph)\nabla M), \quad (3)$$

where $a_{31}(\aleph)$ is the permeability divided by dynamic viscosity; the coupling terms $\nabla \cdot (a_{32}(\aleph)\nabla T)$ and $\nabla \cdot (a_{33}(\aleph)\nabla M)$ describe pressure changes induced by thermal expansion and moisture-induced swelling/shrinkage.

A defining characteristic of this model is that all transport coefficients—$a_{11}, a_{12}, a_{13}, a_{21}, a_{22}, a_{23}, a_{31}, a_{32}, a_{33}$—are explicit functions of the spatial coordinate $\aleph$.

At the initial time $t = 0$:

$$T(\aleph, 0) = T_0(\aleph), \;\; M(\aleph, 0) = M_0(\aleph), \;\; P(\aleph, 0) = P_0(\aleph), \;\; \aleph \in \Omega. \quad (4)$$

We consider mixed boundary conditions (for the parallelepiped cotton pile) that model the exchange of heat, moisture, and momentum with the surrounding atmosphere, which is characterized by a temperature $T_E(t)$, moisture content $M_E(t)$, and pressure $P_E(t)$.

On boundary conditions $\partial\Omega_T$ for heat exchange:

$$-\lambda_T \frac{\partial T}{\partial n} = h_T(T(\aleph, t) - T_E(t)) - q_{Solar}(t), \;\; \aleph \in \partial\Omega_T \quad (5)$$

where h_T is the convective heat transfer coefficient, n is the outward unit normal vector, and $q_{Solar}(t)$ is the incident solar heat flux (which may be zero on shaded faces).

On boundary conditions $\partial\Omega_M$ for moisture exchange:

$$-\lambda_M \frac{\partial M}{\partial n} = h_M(M(\aleph, t) - M_E(t)), \;\; \aleph \in \partial\Omega_M \quad (6)$$

where h_M is the surface moisture transfer coefficient.

Boundaries are exposed to open air, with all lateral faces and the top, but the bottom is treated as impermeable.

On boundary conditions $\partial\Omega_P$ for pressure exchange:

$$-\lambda_P \frac{\partial P}{\partial n} = h_P(P(\aleph, t) - P_E(t)), \;\; \aleph \in \partial\Omega_P \quad (7)$$

where h_P is a pressure exchange coefficient related to the surface porosity.

The boundary segments may overlap or cover the entire boundary, depending on the physical setup.

The complete problem is therefore defined as follows: find the functions $T(\aleph, t)$, $M(\aleph, t)$, and $P(\aleph, t)$ in the domain $\Omega \times \left[0, t_{final}\right]$ that satisfy the coupled nonlinear system of time-fractional PDEs (1)–(3) with spatially variable coefficients, subject to the initial conditions (4) and the mixed boundary conditions (5)–(7).

3. Numerical Solution Algorithm

For solving the coupled, time-fractional, three-dimensional problem, a robust and efficient numerical scheme was developed. The primary challenges are the non-local nature of the Caputo fractional derivative; the strong coupling between temperature (T), moisture (M), and pressure (P) fields; spatially variable coefficients representing material heterogeneity; and the three-dimensional spatial domain. To address these, we develop a high-order finite-difference scheme based on an ADI approach, which decomposes the complex 3D problem into a sequence of simpler one-dimensional sub-problems.

Temporal discretization of the fractional derivative:

Let the total simulation time t_{final} be divided into N_t equal steps of size $\Delta t = t_{final}/N_t$, with discrete times $t^n = n\Delta t$ for $n = 0, 1, \ldots, N_t$. We denote the numerical approximation of a field $u(\aleph, t)$ at grid point $(i,\ j,\ k)$ and time level n as $u^n_{i,j,k}$.

The Caputo fractional derivative of order α $(0 < \alpha \leq 1)$ is approximated using the $L1$-scheme, which provides first-order accuracy in time and is stable for this class of problems [30]. For a function $u(t)$, the discrete approximation at time t^n is

$$\frac{\partial^\alpha u(t^n)}{\partial t^\alpha} \approx \frac{1}{\Gamma(2-\alpha)\Delta t^\alpha} \sum_{m=0}^{n-1} b_m \left(u^{n-m}_{i,j,k} - u^{n-m-1}_{i,j,k} \right) \ , \ n \in (0,\ N_t), \tag{8}$$

where the weights b_m are given by

$$b_m = (1+m)^{1-\alpha} - m^{1-\alpha}, \ \ 0, 1, \ldots, n-1. \tag{9}$$

The spatial domain $\Omega = [0, L_x] \times [0, L_y] \times [0, L_z]$ is discretized using a uniform grid with N_x, N_y, N_z points in the x, y, z directions, respectively. The grid spacings are $\Delta x = L_x/(N_x - 1)$, $\Delta y = L_y/(N_y - 1)$, $\Delta z = L_z/(N_z - 1)$.

This transforms the 3D implicit problem, which would require solving a very large sparse system, into three sequential 1D problems, each solvable via an efficient tridiagonal matrix algorithm.

For a generic coupled equation of the form:

$$\frac{\partial^\alpha u}{\partial t^\alpha} = \nabla \cdot (A(\aleph)\nabla u) + \nabla \cdot (B(\aleph)\nabla v) + \nabla \cdot (C(\aleph)\nabla w) + S, \tag{10}$$

we apply the following fractional ADI splitting over one full time step from t^n to t^{n+1}:

Sub-step 1: Solve in the x-direction (implicit in x, explicit in y, z):

$$\frac{1}{\Gamma(2-\alpha)\Delta t^\alpha} \sum_{m=0}^{n} b_m \left(u^{n+\frac{1}{3}} - u^{n-m} \right) = \delta_x \left(A\delta_x u^{n+\frac{1}{3}} \right) + \delta_x (B\delta_x v^n) + \delta_x (C\delta_x w^n) + \delta_y \left(A\delta_y u^n \right) + \delta_z (A\delta_z u^n) + S^n, \tag{11}$$

where $\delta_x, \delta_y, \delta_z$ denote centered finite-difference approximations of the spatial derivatives.

Sub-step 2: Solve in the y-direction (implicit in y, explicit in x, z) using the result from Step 1:

$$\frac{1}{\Gamma(2-\alpha)\Delta t^{\alpha}}\sum_{m=0}^{n} b_m\left(u^{n+\frac{2}{3}}-u^{n-m}\right)=\delta_y\left(A\delta_y u^{n+\frac{2}{3}}\right)+\delta_x\left(B\delta_x v^{n+\frac{1}{3}}\right)+\delta_x\left(C\delta_x w^{n+\frac{1}{3}}\right)+\delta_x\left(A\delta_x u^{n+\frac{1}{3}}\right)+\delta_z\left(A\delta_z u^{n+\frac{1}{3}}\right)+S^{n+\frac{1}{3}}, \quad (12)$$

Sub-step 3: Solve in the z-direction (implicit in z, explicit in x, y) to obtain the final solution at t^{n+1}:

$$\frac{1}{\Gamma(2-\alpha)\Delta t^{\alpha}}\sum_{m=0}^{n} b_m\left(u^{n+1}-u^{n-m}\right)=\delta_z\left(A\delta_z u^{n+1}\right)+\delta_x\left(B\delta_x v^{n+\frac{2}{3}}\right)+\delta_x\left(C\delta_x w^{n+\frac{2}{3}}\right)+\delta_x\left(A\delta_x u^{n+\frac{2}{3}}\right)+\delta_y\left(A\delta_y u^{n+\frac{2}{3}}\right)+S^{n+\frac{2}{3}}, \quad (13)$$

The coupling terms involving gradients of the other fields (v, w) and the variable coefficients are treated explicitly at the known time level to maintain linearity in each sub-step.

A critical aspect for accuracy in heterogeneous media is the evaluation of spatially variable coefficients at cell interfaces. We employ harmonic averaging to ensure flux continuity. For example, the coefficient $A(x)$ at the interface $i+1/2$ is approximated as

$$A_{i+1/2,\,j,k}=\frac{2A_{i,j,k}A_{i+1,j,k}}{A_{i,j,k}+A_{i+1,j,k}} \quad (14)$$

This approach is physically consistent, as it preserves the correct effective conductivity between dissimilar materials.

The three systems (for T,M,P) are solved in a segregated manner within each ADI sub-step. That is, we first solve the entire ADI cycle for T while keeping M and P fixed at the previous time level, then solve for M using the updated T, and finally solve for P using the updated T and M. This segregated approach is iterated within each physical time step until convergence of the coupled system is achieved (typically 2–3 iterations suffice due to the small-time step).

For the boundary conditions, (5)–(7) are incorporated into the finite-difference stencil at the boundary nodes. For the left boundary in x (i = 0), condition (5) is discretized as

$$-\lambda_T\frac{-3T_{0,j,k}^{n+\frac{1}{3}}+4T_{1,j,k}^{n+\frac{1}{3}}-T_{2,j,k}^{n+\frac{1}{3}}}{2\Delta x}=h_T\left(T_{0,j,k}^{n+\frac{1}{3}}-T_E^{n}\right)-q_{Solar}^{n}(t), \quad (15)$$

This equation is rearranged to express the ghost node value or, more efficiently, is used to modify the coefficients of the tridiagonal system for the first interior node, ensuring the boundary condition is satisfied implicitly. The converged solution T^{n+1}, M^{n+1}, P^{n+1} is appended to the time–history array required for the fractional derivative computation at the next step.

The major computational cost stems from two factors: the $O(N_t^2)$ memory and operation count for the direct evaluation of the fractional derivative sum in (8) and the need to solve three tridiagonal systems per field per ADI sub-step. For long-time simulations, the history cost can be mitigated using the "short memory" principle or fast convolution algorithms.

4. Results and Discussion

The numerical model was employed to simulate the coupled heat–moisture transfer with gas flow within a large parallelepiped cotton storage pile (12 × 20 × 8 m) over an extended period of 30 days under open-air conditions. Based on agricultural engineering and the textile research literature, we used the following key coefficients for raw cotton: density (ρ): 65 kg/m^3 (bulk density of cotton bale); specific heat capacity (c): 1400 J/kg·K; thermal conductivity (a_{11}): 0.05 W/m·K, which was highly dependent on moisture content and compression—moisture content is reported on a wet basis as $M_{wb}(\%) = \frac{m_w}{m_w+m_s}100$, where m_w is the mass of water and m_s is the dry-solid mass; equilibrium moisture content (EMC): 6–8% at 20 °C, 65%

RH; moisture diffusivity (a_{21}): 1.0×10^{-9} to 1.0×10^{-8} m^2/s; air permeability (κ): 0.5–2.0 $\times 10^{-7}$ m^2; porosity (ε) is assumed constant: 0.85–0.95; compressibility (a_{31}): 0.7–1.0 $\times 10^{-5}$ Pa^{-1}; thermo-moisture (a_{12}): 0.65–1.0 $\times 10^{-7}$ W·s/kg·m; thermo-pressure (a_{13}): 0.45–1.0 $\times 10^{-10}$ W·s/Pa·m; moisture–thermal (a_{22}): 0.75–1.0 $\times 10^{-10}$ m^2/s·K; moisture–pressure (a_{23}): 0.8–1.0 $\times 10^{-12}$ m^2/s·Pa; pressure–thermal (a_{32}): 0.5–1.0 $\times 10^{-12}$ m^2/s·K; pressure–moisture (a_{33}): 0.75–1.0 $\times 10^{-10}$ m^2/s; heat transfer coefficient (h_T): 15 W/m^2·K; mass transfer coefficient (h_M): 0.02 m/s; pressure exchange coefficient (h_P): 0.001 m/s; and solar absorptivity (α_s): 0.7 for cotton raw. The fractional order $\alpha = 0.75$ was identified from experimental/benchmark data by minimizing the discrepancy between simulated and measured responses.

The analysis focuses on 15 days (mid-term) and 30 days (long-term) of storage, corresponding to typical storage durations for raw cotton piles as a parallelepiped domain (consistent with the pile geometry used in practice).

After 15 days of storage, the diurnal temperature cycle established a quasi-steady pattern, with surface layers experiencing fluctuations of ±6–8 °C, while the core remained relatively stable (Figure 1). The average temperature was 24.8 °C, where the maximum temperature was 37.8 °C in the central region at a 2.5 m depth (Figure 1). The heat release rate was 0.08–0.15 W/m^3 in moist regions. The system at 15 days demonstrated that under favorable environmental conditions (average 25 °C, 65% RH), cotton can be stored safely with minimal risk. The fractional model captures the gradual moisture redistribution from the bottom to top regions, a phenomenon that would be underestimated by classical integer-order models.

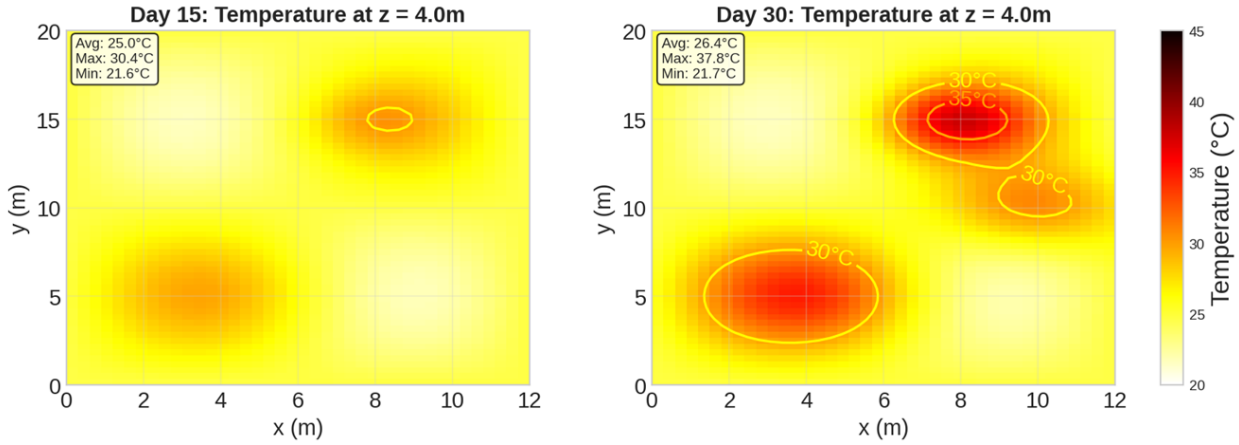


Figure 1. Comparative analysis of temperature change.

By day 15, cumulative effects of environmental exposure and internal moisture release activity became significant (Figure 2). A simulated rain event on day 12 (0.8 intensity) introduced additional moisture, creating localized regions of concern. Moisture-dependent heating in local temperature increases of 2–3 °C can be attributed to microbial activity. The fractional model's memory effect correctly predicts the persistence of moisture in certain regions.

By day 30, the average moisture content (% wet basis) was 11.1% (+4.1% from initial), where the maximum moisture content was at 18.2%, which is the critical level for microbial growth. Pressure gradients were up to 85 Pa/m, sufficient for weak convection.

Risk escalation was linear for the first 15 days (0.2 points/day), then accelerated to 0.4 points/day (Figure 3). The time-dependent risk evolution for days 0–15 was low risk (score 0–2) and needed sufficient standard monitoring. For days 15–22, it was moderate risk (score 3–4), and increased vigilance was needed; for days 22–30 of storage, it was high

risk (score 5–6), and active intervention was required. Beyond 30 days was critical risk (score 7–10), with significant quality loss being likely (Figure 3).

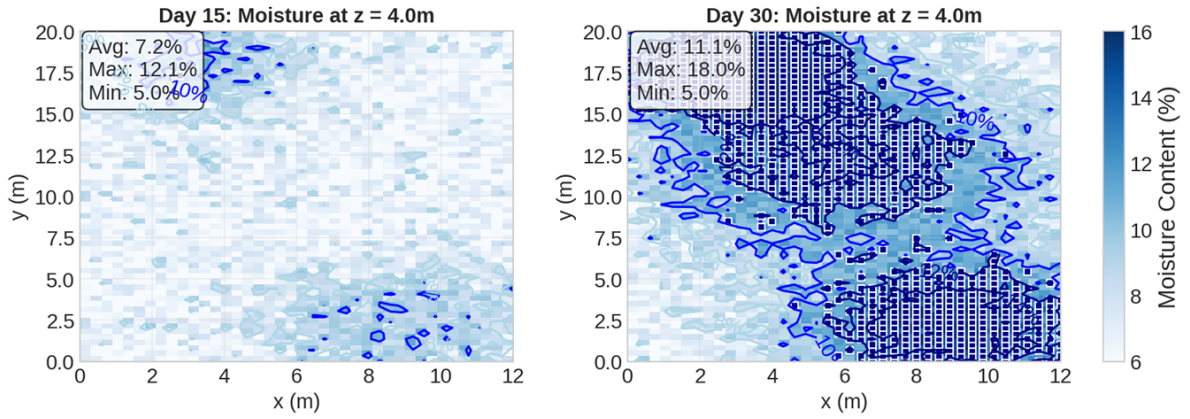


Figure 2. Comparative analysis of moisture change.

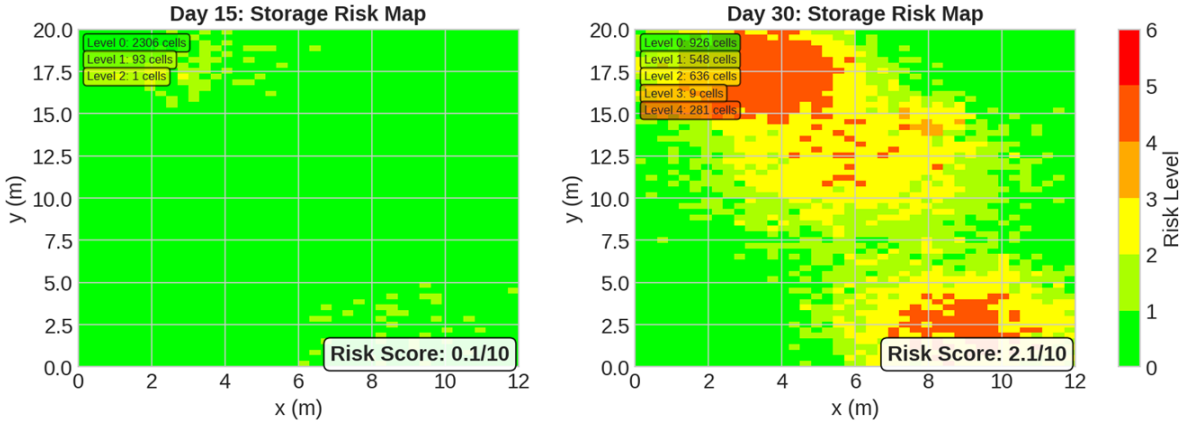


Figure 3. Comparative analysis of risk evolution.

Clear upward migration occurred due to thermal gradients, with the bottom layers losing 0.5–1.0% moisture to upper regions (Figure 4). The average moisture content was 9.2% (+0.5% from day 15) and the maximum moisture content was 13.8%. Moisture stratification showed a clear vertical pattern with a 3.5% difference between the top and bottom (Figure 4).

Temperature oscillations had an amplitude of 12 °C in the surface layers and 4 °C in the core, where the maximum temperature was 46.3 °C in the deep central region at a depth of 4.2 m (Figure 5). The average temperature increase rate was 0.12 °C/day (linear) but reached a maximum of 0.35 °C/day (exponential). Quality loss estimate was 2–3% at 15 days and 8–12% at 30 days. The optimum storage duration was 12–20 days under these conditions before significant quality loss.

Field measurements during the autumn compared with the developed and Mamatov models [14] generally confirmed the results of numerical calculations. The likelihood of a self-heating effect increased in proportion to the increase in the moisture and density of cotton storage. When the raw cotton's average initial temperature and moisture were 29 °C and 30.7% (wet basis), respectively (Figure 6), in certain areas, then over the next 30 days, the temperature gradually increased because of internal and external influence.

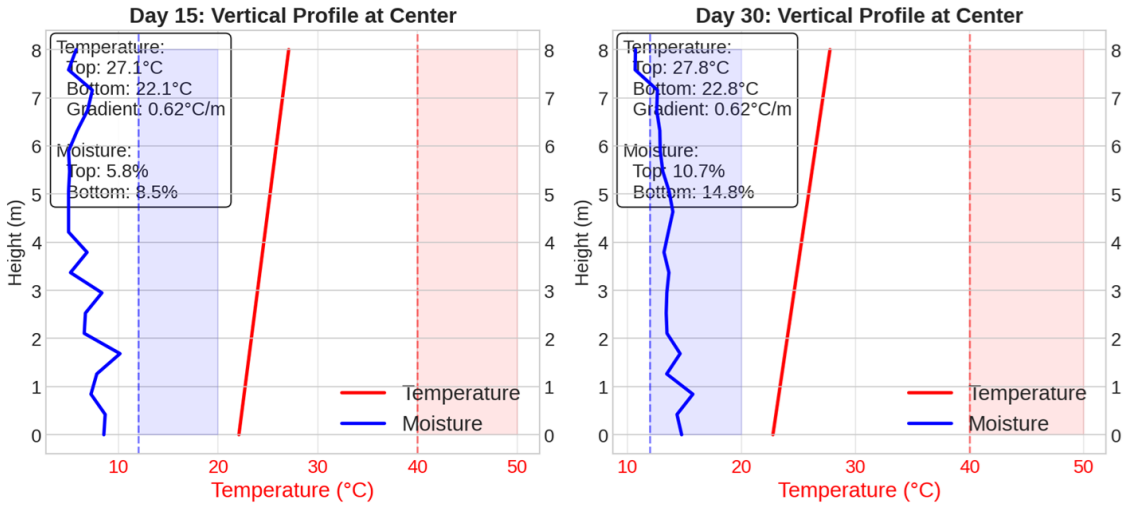


Figure 4. Vertical profiles through cotton raw storage.

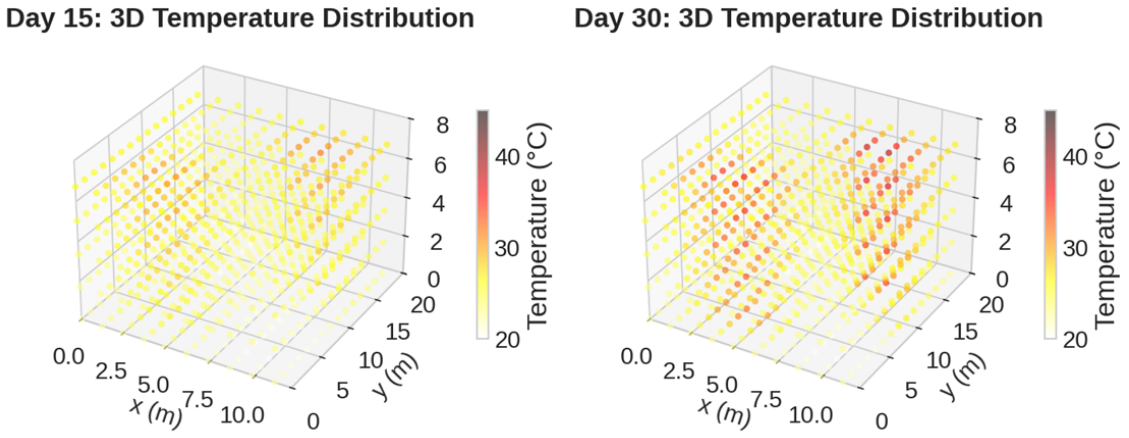


Figure 5. Temperature distribution in raw cotton.

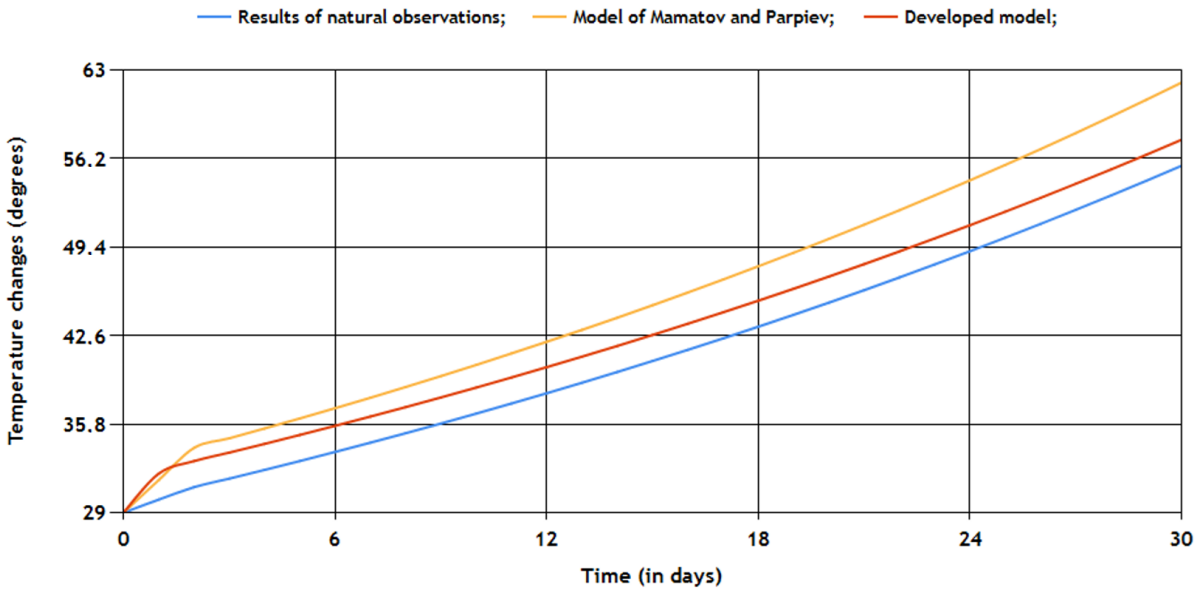


Figure 6. Average temperature content after 30 days of storage in open areas.

The performed validation demonstrated that the developed coupled model, with physically justified parameters and boundary conditions matching the long-term storage regime, is capable of reliably predicting the spatial–temporal evolution of temperature with

a high content of moisture (30.7% wet basis) in 30 days (Figure 7) of stored raw cotton. It was implemented in Kagan and Peshku Cotton Cleaning JSC facilities. The agreement with monitoring data and the stability of predictions under parameter variations collectively confirm the adequacy of the model for analyzing raw cotton long-term storage conditions.

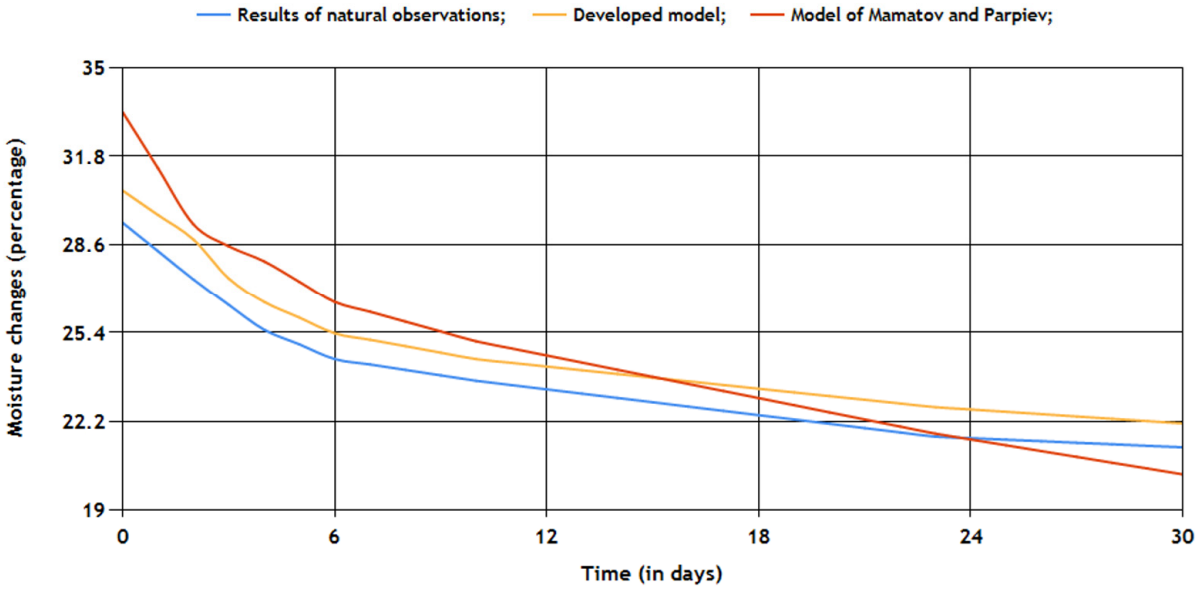


Figure 7. Average moisture content after 30 days of storage in open areas.

5. Conclusions

This research has developed and implemented a novel fractional calculus-based framework for simulating the interconnected transport mechanisms of thermal energy, moisture content, and pressure within large-scale raw cotton storage and drying operating under ambient atmospheric conditions. The same formulation is applicable to food materials (e.g., grains, fruits) as hygroscopic porous media. Employing Caputo fractional derivatives with an exponent parameter of $\alpha = 0.75$ provided an effective mathematical representation of the memory-dependent phenomena and anomalous diffusion patterns observed in raw cotton over extended temporal scales in storage environments.

In terms of the simulation results obtained under standard open-air storage parameters (27 °C ambient temperature with 56% relative humidity), the analysis indicates that cotton should not remain in storage beyond 30 days without implementing active environmental control measures. In the long-term (day 45) storage of raw cotton, the average moisture content was 18.1% and the maximum moisture content was at 25.2%, which are critical levels for safe storage. Exceeding this duration threshold may result in quality degradation exceeding 9%.

This computational model provides enhanced forecasting accuracy of temperature, moisture, and pressure variations across extended storage periods, thereby facilitating preemptive management of storage and drying conditions that affect product quality and safety. Consequently, the implementation of this predictive framework could potentially yield loss reduction, like burning or rotting the quality of the fiber, with benefits of 20–30% relative to conventional monitoring approaches. The reliability of the research results is substantiated by the fact that the heat and moisture transfer equations are formulated in strict accordance with the laws of conservation and transfer of mass, energy, and momentum, as well as the agreement of the results of numerical calculations with experimental data. Finally, models where the fractional order α varies with time, space, and material properties will be involved in the future to better capture evolving transport characteristics.

Author Contributions: Conceptualization, N.R. and I.S.; methodology, N.R. and I.S.; software, I.S.; validation, N.R. and I.S.; formal analysis, I.S.; investigation, I.S.; resources, I.S.; data curation, I.S.; writing—original draft preparation, I.S.; writing—review and editing, I.S.; visualization, I.S.; supervision, N.R. project administration, I.S.; funding acquisition, I.S. All authors have read and agreed to the published version of the manuscript.

Funding: This research received no external funding.

Data Availability Statement: All data needed to support the findings of this research are included within the article.

Conflicts of Interest: The authors declare no conflicts of interest.

References

1. Khan, M.I.H.; Batuwatta-Gamage, C.P.; Karim, M.A.; Gu, Y. Fundamental Understanding of Heat and Mass Transfer Processes for Physics-Informed Machine Learning-Based Drying Modelling. *Energies* **2022**, *15*, 9347. [CrossRef]
2. Ozarslan, R.; Bas, E. Kinetic Model for Drying in Frame of Generalized Fractional Derivatives. *Fractal Fract.* **2020**, *4*, 17. [CrossRef]
3. Shadmanov, I.; Shafiyev, T. Mathematical modeling of the processes of combined heat and moisture transfer during storage and drying of raw cotton. *E3S Web Conf.* **2023**, *431*, 01060. [CrossRef]
4. Philip, J.R.; De Vries, D.A. Moisture movement in porous materials under temperature gradients. *Eos Trans. Am. Geophys. Union* **1957**, *38*, 222–232. [CrossRef]
5. Luikov, A.V. Systems of differential equations of heat and mass transfer in capillary-porous bodies (review). *Int. J. Heat Mass Transf.* **1975**, *18*, 11–24. [CrossRef]
6. Liu, J.Y. Drying of Porous Materials in a Medium with Variable Potentials. *J. Heat Transf.* **1991**, *113*, 757–762. [CrossRef]
7. Pandey, R.N.; Srivastava, S.K.; Mikhailov, M.D. Solutions of Luikov equations of heat and mass transfer in capillary porous bodies through matrix calculus: A new approach. *Int. J. Heat Mass Transf.* **1999**, *42*, 2649–2660. [CrossRef]
8. Patankar, S.V. *Numerical Heat Transfer and Fluid Flow*; CRC Press: Boca Raton, FL, USA, 2018; pp. 67–84. [CrossRef]
9. Whitaker, S. Simultaneous Heat, Mass, and Momentum Transfer in Porous Media: A Theory of Drying. *Adv. Heat Transf.* **1977**, *13*, 119–203. [CrossRef]
10. Berkowitz, B.; Cortis, A.; Dentz, M.; Scher, H. Modeling non-Fickian transport in geological formations as a continuous time random walk. *Rev. Geophys.* **2006**, *44*, RG2003. [CrossRef]
11. Nield, D.A.; Bejan, A. Heat Transfer Through a Porous Medium. In *Convection in Porous Media*; Springer International Publishing: Cham, Switzerland, 2017; pp. 37–55. [CrossRef]
12. Ranjbarzadeh, R.; Sappa, G. Numerical and Experimental Study of Fluid Flow and Heat Transfer in Porous Media: A Review Article. *Energies* **2025**, *18*, 976. [CrossRef]
13. Khan, F.A.; Straatman, A.G. A conjugate fluid-porous approach to convective heat and mass transfer with application to produce drying. *J. Food Eng.* **2016**, *179*, 55–67. [CrossRef]
14. Mamatov, A.; Parpiev, A.; Kayumov, A. Mathematical models of the heat and mass exchange process during pneumo-transportation of cotton-raw. *Theor. Appl. Sci.* **2020**, *91*, 508–514. [CrossRef]
15. Wang, H.; Lu, T.; Zhang, Q. Drying characteristics of biological porous media during convective drying. *Int. J. Agric. Biol. Eng.* **2016**, *9*, 194–207. [CrossRef]
16. Adizova, Z.; Shadmanov, I. Mathematical modeling of heat and moisture exchange processes for grain storage. *AIP Conf. Proc.* **2024**, *3244*, 020042. [CrossRef]
17. Sorokova, N.; Didur, V.; Variny, M. Mathematical Modeling of Heat and Mass Transfer during Moisture–Heat Treatment of Castor Beans to Improve the Quality of Vegetable Oil. *Agriculture* **2022**, *12*, 1356. [CrossRef]
18. Mozafarifard, M.; Toghraie, D. Numerical analysis of time-fractional non-Fourier heat conduction in porous media based on Caputo fractional derivative under short heating pulses. *Heat Mass Transf.* **2020**, *56*, 3035–3045. [CrossRef]
19. Kilbas, A.A.; Srivastava, H.M.; Trujillo, J.J. Preface. In *Theory and Applications of Fractional Differential Equations*; Elsevier: Amsterdam, The Netherlands, 2006; pp. 12–32. [CrossRef]
20. Sokolovskyy, Y.; Drozd, K.; Samotii, T.; Boretska, I. Fractional-Order Modeling of Heat and Moisture Transfer in Anisotropic Materials Using a Physics-Informed Neural Network. *Materials* **2024**, *17*, 4753. [CrossRef]
21. Metzler, R.; Klafter, J. The random walk's guide to anomalous diffusion: A fractional dynamics approach. *Phys. Rep.* **2000**, *339*, 1–77. [CrossRef]
22. Atangana, A.; Baleanu, D. New fractional derivatives with nonlocal and non-singular kernel: Theory and application to heat transfer model. *Therm. Sci.* **2016**, *20*, 763–769. [CrossRef]

23. Navarro, M.C.; Castaño, D.; Herrero, H. Growing Top-Down or Bottom-Up Vortices: Effect of Thermal Gradients. *Modelling* **2025**, *6*, 166. [CrossRef]
24. Ndukwu, M.; Ibeh, M.; Ekop, I.; Abada, U.; Etim, P.; Bennamoun, L.; Abam, F.; Simo-Tagne, M.; Gupta, A. Analysis of the Heat Transfer Coefficient, Thermal Effusivity and Mathematical Modelling of Drying Kinetics of a Partitioned Single Pass Low-Cost Solar Drying of Cocoyam Chips with Economic Assessments. *Energies* **2022**, *15*, 4457. [CrossRef]
25. Ravshanov, N.; Shadmanov, I.U. Multidimensional model of heat-moisture transport in porous media. *J. Phys. Conf. Ser.* **2020**, *1546*, 012098. [CrossRef]
26. Lin, Y.; Xu, C. Finite difference/spectral approximations for the time-fractional diffusion equation. *J. Comput. Phys.* **2007**, *225*, 1533–1552. [CrossRef]
27. Diethelm, K. *The Analysis of Fractional Differential Equations*; Springer: Berlin/Heidelberg, Germany, 2010; Volume 2004, p. 216. [CrossRef]
28. Li, C.; Zeng, F. *Numerical Methods for Fractional Calculus*; Chapman and Hall/CRC: Boca Raton, FL, USA, 2015; p. 45. [CrossRef]
29. Jumaev, J.; Bozorov, Z.; Shadmanov, I.; Atoev, D. Investigation of initial-boundary value problem for integro-differential fractional diffusion equation. *AIP Conf. Proc.* **2024**, *3004*, 040004. [CrossRef]
30. Yang, T.; Liu, L.-B.; Bao, X.; Zhang, Y. An Optimal Adaptive Grid Method Based on L1 Scheme for a Nonlinear Caputo Fractional Differential Equation. *Fractal Fract.* **2022**, *6*, 647. [CrossRef]

Disclaimer/Publisher's Note: The statements, opinions and data contained in all publications are solely those of the individual author(s) and contributor(s) and not of MDPI and/or the editor(s). MDPI and/or the editor(s) disclaim responsibility for any injury to people or property resulting from any ideas, methods, instructions or products referred to in the content.